EXOTIC MESONS WITH NON−$q\bar{q}$ QUANTUM NUMBERS

W. Dünnweber

Sektion Physik, Universität München, D-85748 Garching

Resonances with exotic quantum numbers give unequivocal evidence for non-$q\bar{q}$ structure. A resonance with exotic quantum numbers $J^{PC} = 1^{-+}$ is observed in the annihilation reactions $\bar{p}n \rightarrow \eta\pi^-\pi^0$ and $\bar{p}p \rightarrow \eta\pi^0\pi^0$. In the highly selective $\bar{p}n$ channel it is produced with a large rate (11%). The interferences with the other two dominant resonances, $\rho(770)$ and $a_2(1320)$, allow to pin down the resonance characteristics: $m = (1400 \pm 20 \pm 20) MeV/c^2$ and $\Gamma = (310 \pm 50^{+50}_{-30}) MeV/c^2$. In $\bar{p}p \rightarrow \eta\pi^0\pi^0$ the exotic resonance is produced with a smaller relative rate ($\sim 1\%$ in liquid hydrogen, 4% in gaseous hydrogen at 12 atm). It is concluded that the resonance is produced more abundantly from spin triplet than from spin singlet states. Comparison with π-induced peripheral reactions yields agreement with the weak $\eta\pi$ resonance observed there. However, the VES and Brookhaven experiments have also produced a $J^{PC} = 1^{-+}$ resonance at higher mass (1600 MeV), decaying to $\eta'\pi, \rho\pi$ and $b_1\pi$. Thus at least two resonances with exotic quantum numbers exist which await modeling in theories of hybrid ($q\bar{q}g$) and diquonium ($qq\bar{q}\bar{q}$) states.

Introduction

Mesons with the exotic quantum numbers $J^{PC} = 0^{--}, 0^{+-}, 1^{-+}, 2^{+-}, \ldots$ have necessarily non-$q\bar{q}$ structure due to the generalized Pauli principle. Glueballs and quark-gluon hybrids, but also diquonia ($qq\bar{q}\bar{q}$) or meson molecules can attain these quantum numbers. Unlike the 0^{++} glueball, mesons with exotic quantum numbers cannot mix with ordinary ($q\bar{q}$) mesons. Thus the identification of a meson with exotic J^{PC} gives unambiguous evidence for other or more constituents than one quark and one antiquark.

The $\eta\pi$ system is attractive for the exotics search since its P-wave must carry non-$q\bar{q}$ quantum numbers $J^{PC} = 1^{-+}(G = -)$. It cannot form a glueball, however, because of its isospin one. In our experiments [1,2] it is produced in the annihilation reactions (at rest)

$$(a)\bar{p}n \rightarrow \eta\pi^-\pi^0, \qquad\qquad (b)\bar{p}p \rightarrow \eta\pi^0\pi^0.$$

Only the atomic S- and P-wave contribute significantly, and conservation rules restrict the initial states to (a) $^3S_1, ^1P_1$ and (b) $^1S_0, ^3P_1, ^3P_2$.

1.   Experimental results for $\bar{p}n \rightarrow \eta\pi^-\pi^0$

Antiprotons with a momentum of 200 MeV/c from the LEAR facility at CERN were stopped in a liquid deuterium target. The Crystal Barrel Detector is equipped for charged particle tracking in a magnetic field of 1.5 T and photon spectroscopy with a highly granular CsI calorimeter, both with close-to-4π geometry.

From a total of 8.2 million 1-prong events, corresponding to about 10^8 $\bar{p}d$ events, a sample of 52576 events of the type $\bar{p}d \rightarrow \pi^-\pi^0(\gamma\gamma)\eta(\gamma\gamma)p$ with a proton spectator momentum < 100 MeV/c was fully reconstructed and kinematically selected. The momentum cut was chosen to guaranty the spectator role of the proton, i.e. the negligibility of final state interactions with the produced mesons [1].

The experimental intensity distribution is displayed as a Dalitz plot in Fig. 1. A simple pattern is observed which is dominated by a diagonal ρ^- (770) band and two broad orthogonal bands in the region of the $a_2^{-/0}$ (1320). The latter show large modulations typical of interference effects.
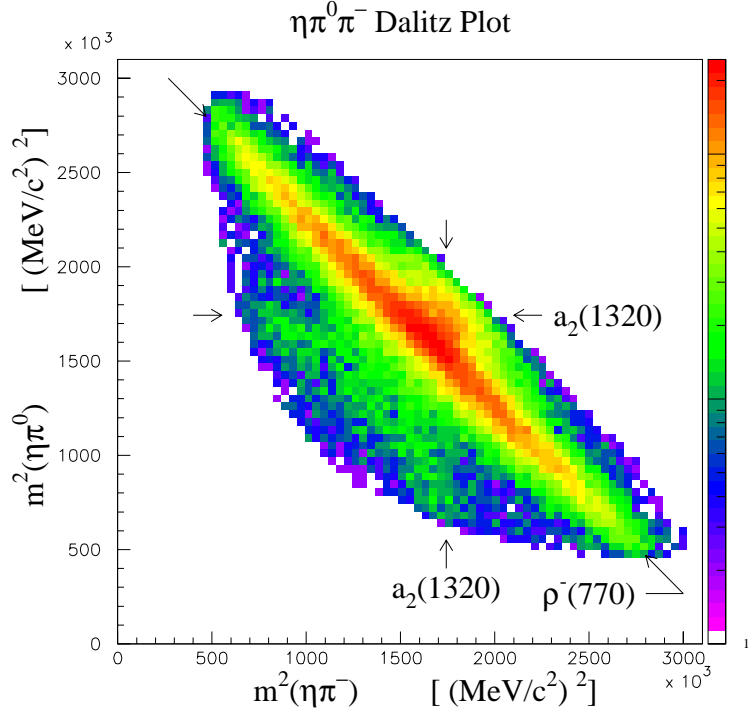
Figure 1. Experimental intensity distribution (binned and acceptance corrected).

2. Partial wave analysis

The partial wave analysis assumes intermediate states of $\pi^-\pi^0$ resonances with a recoiling η or $\eta\pi$ resonances with a recoiling π:

All allowed known or candiate resonances (see above) with nominal mass inside or close to the phase space boundary were tried. The isobar transition amplitude is expressed by use of the Zemach formalism (see [1] and references given there). For an intermediate state decaying into 2 pseudoscalars with angular momentum ℓ, the amplitude for the transition of an initial $\bar{p}n$ state with quantum numbers I^G, J^P into a 3-body channel reads

$$A_{I^G,J^P}(\vec{p},\vec{q}) = \sum_{I_3,L} b_{I,I_3} \cdot Z_{J^P,\ell,L}(\vec{p},\vec{q}) \cdot F_{I_3,\ell}(\vec{q}).$$

The spin-parity function Z describes the dependence on the angle between the decay momentum vectors $\vec{p}$ and $\vec{q}$ of the intermediate and of the secondary two-body systems, respectively. The isospin Clebsch-Gordon coefficients are $b_{1,0} = 1/\sqrt{2}$ and $b_{1,-1} = -1/\sqrt{2}$ for the $\eta\pi^0$ and the $\eta\pi^-$ intermediate systems, respectively. The dynamical amplitude F is factorized into a barrier-penetration factor B_ℓ (q) and a relativistic Breit-Wigner amplitude

$$F = \alpha \cdot D_L(p, p_0) \cdot \frac{m_0 \Gamma_0 D_\ell(q, q_0)/\rho(m_0)}{m_0^2 - m^2 - im_0 \cdot \Gamma(m)} \tag{1}$$

with mass dependent width

$$\Gamma(m) = \Gamma_0 \frac{\rho(m)}{\rho(m_0)} D_\ell(q, q_0)^2, \tag{2}$$

$$(\rho = 2q/m, D_\ell(q, q_0) = B_\ell(q)/B_\ell(q_0)).$$

The complex constant α is optimized by the fit.

A simple model space containing only the $\rho^-(770)\eta, a_2(1320)\pi$ and $(\eta\pi)_{P-wave}\pi$ intermediate states is sufficient for a good fit ($\chi^2/N_{dof} = 506/391$). The contribution of the exotic $\eta\pi$ resonance (baptized $\hat{\rho}$ or π_1) amounts to 11% (without the interferences with the other two resonances), which is about as much as the a_2 contribution. Without the $\eta\pi$ P-wave no satisfactory fits are obtained and the χ^2 distribution gives evidence for missing interference structure (Fig. 2). Inclusion of the $\eta\pi$ P-wave yields a flat χ^2 distribution with only statistical fluctuations [1].
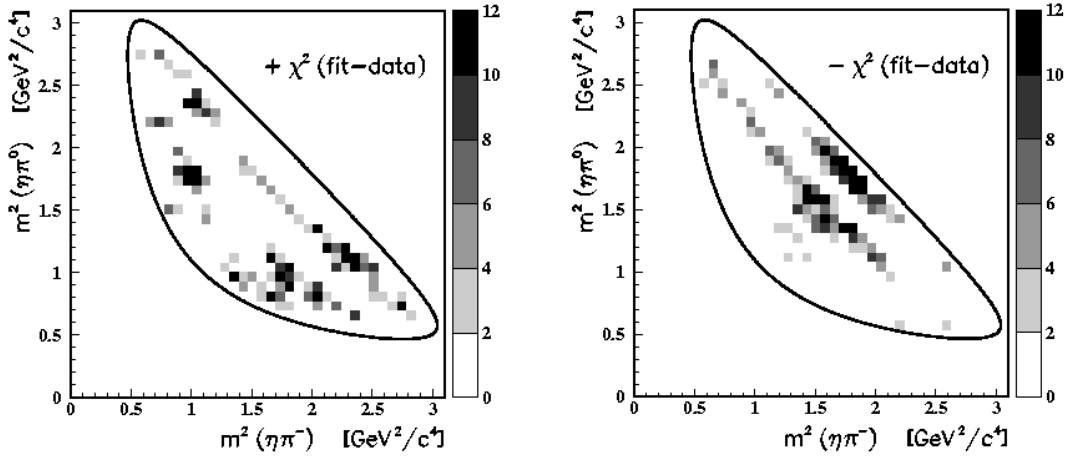

Figure 2. Deviations between the data and a fit that does not include the $\eta\pi$ P-wave but all other allowed resonances. Left panel: fit exceeds data, right panel: reverse.

3. Discussion and comparison with $\bar{p}p \to \eta\pi^0\pi^0$

The interference of the $\eta\pi$ P-wave with both the ρ^- and the a_2 resonances pins down the resonance characteristics. The relative phase of the latter two resonances is fixed by their crossing in the Dalitz plot. Both probe the $\eta\pi$ phase motion in different regions. Constructive and destructive interference on opposite sides of the ρ^- band center is visible in Fig. 3 which shows the intensity distribution of the exotic resonance including the interferences. Moving along a parallel just below the position of the ρ^- band, one observes the rise and the fall of the constructive term, which reflects the almost complete phase rotation of the $\eta\pi$ resonance. Close to the phase space boundaries, one finds at $m^2(\eta\pi) = (1.7 - 1.8)$ GeV$^2/c^4$ the interference maximum and minimum arising from the overlap with the a_2.

Figure 3. Intensity distribution of the $\eta\pi$P-wave, as obtained by subtracting from the experimental intensity the ρ^- and a_2 contributions according to the partial wave analysis.
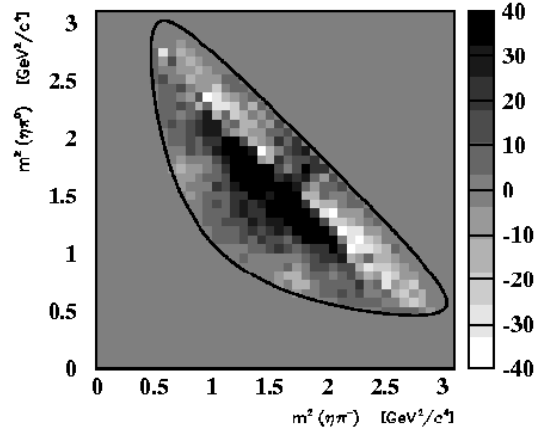
The fitted parameters of the exotic resonance are

$$M = (1400 \pm 20_{stat} \pm 20_{syst})\,MeV/c^2, \qquad \Gamma = (310 \pm 50_{stat} + 50/-30_{syst})\,MeV/c^2.$$

These values are not inconsistent with the GAMS [3] and VES [4] results for pion-induced reactions and they agree with the BNL results [5] obtained at the same time as the present ones. In those cases the relative contribution from the $\eta\pi$ wave is much smaller and the evidence is based only on interferences with the a_2.

As an alternative model of the $\eta\pi$ P-wave, an effective range amplitude is found to yield convergent or divergent fits in the range of scattering parameters that characterize resonant or nonresonant behaviour, respectively. The resonant solution is practically identical to the Breit-Wigner fit amplitude. Its phase motion shows the typical resonance behaviour in an Argand diagram (Fig. 4). It is evident from this representation that the complete phase motion is probed in the present Dalitz plot.
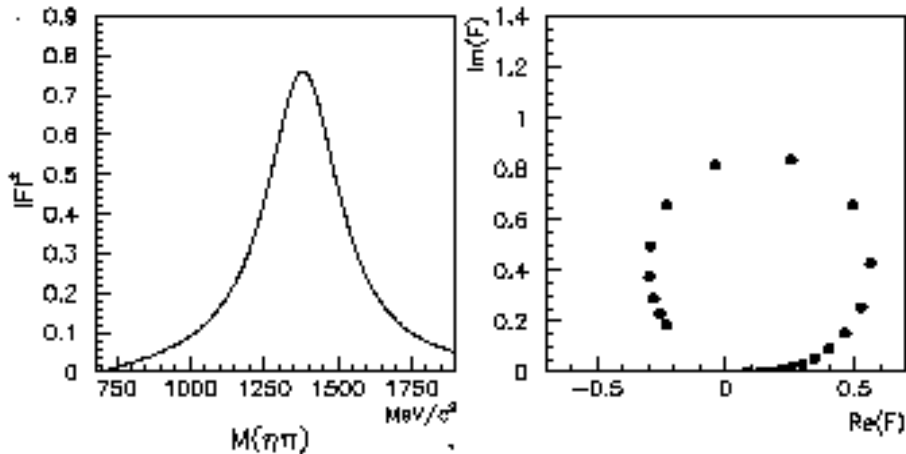

Figure 4. Lhs: $(\eta\pi)_P$ effective range amplitude (squared absolute value) fitted to the data. Rhs: Corresponding Argand plot, showing the imaginary versus the real part of the effective range amplitude. The range from M = 690 to 1800 MeV/c^2 is divided into equal Δm steps. An almost complete anticlockwise phase rotation is observed.

We have also studied the so-called cusp effect which arises from the opening of another channel under a broad resonance, thus creating an apparently narrower structure. Since additional 1^{-+} structure is indicated in the $\rho\pi$ system in the mass range 1600-1700 MeV/c^2 [6, 7], we have investigated the possibility that a broad resonance in that range produces a cusp at 1400 MeV/c^2 in $\eta\pi$, using the Flatté parametrization [8]. However, the corresponding fits fail. The high statistics of the Crystal Barrel data allow a distinction of the different shapes of a cusp (Fig. 5) and a Breit-Wigner resonance (cf. Fig.4). As a function of the mass m_1 of the broad resonance, the cusp fits clearly get worse with increasing m_1 (Fig. 6). The minimum χ^2 is reached at $m_1 = 1400$ MeV/c^2 which is identical to the mass of the Breit-Wigner fit. However at this minimum, the value of χ^2 is still worse by $\Delta\chi^2 = 42$ than the corresponding value for the Breit-Wigner fit. It is concluded that the resonance at 1400 MeV/c^2 is not a cusp from the resonance at higher mass observed at VES and Brookhaven. Consistency of all observations is obtained with two resonances, one at 1400 MeV/c^2, the other at about 1600 MeV/c^2.
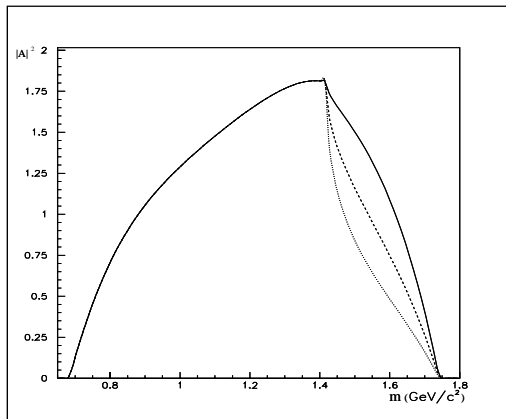

Figure 5. Calculated cusp amplitude for a broad exotic $\eta\pi$ resonance at 1600 MeV/c^2 coupled to the $f_1\pi$ system (threshold at 1420 MeV/c^2). The Flatté parametrization is used where the width $\Gamma(m)$ in eqs. (1,2) is replaced by $\Gamma_{\eta\pi}(m) + 2(q_{f_1\pi}/m)\cdot\Gamma_{0,f_1\pi}$. Plotted is the squared magnitude of the amplitude for $\Gamma_{0,\eta\pi} = 1000$ MeV/c^2 and $\Gamma_{0,f_1\pi} = 300, 1000, 2000$ MeV/c^2 (from top to bottom, respectively) [9].
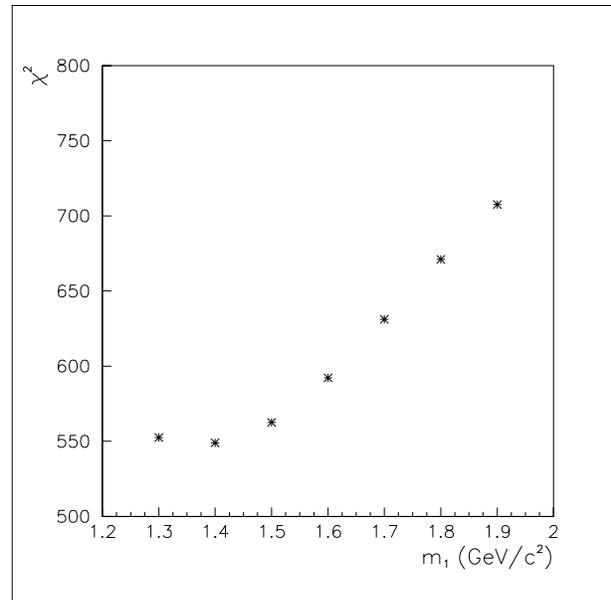
Figure 6. Deviation of cusp fits from data (χ^2) as a function of the mass of a broad $(\Gamma_{0,\eta\pi} = 1000 MeV/c^2)$ exotic $\eta\pi$ resonance with fitted width $\Gamma_{0,f_1\pi}$, using the Flatté parametrization (see Fig. 5).

Finally, an interesting entrance channel selectivity is found when the above $\bar{p}n$ data are compared to $\bar{p}p$. In that case the Dalitz plot is very rich in structure (Fig. 7) and the evidence for a contribution of the exotic resonance could only be obtained by coupled analysis of data for a liquid and a gaseous hydrogen target [2]. With the latter target, the relative contribution from the atomic P-state is enhanced. The analysis yields relative contributions of the exotic resonance of 1% and 4% for the liquid and the gaseous target, respectively, and resonance parameters consistent with the values given above. Here the dominant contribution comes from the atomic $^3P_1$ state. The $^1S_0$ state is strongly suppressed, in contrast to the dominance of the $^3S_1$ state in $\bar{p}$n. Hence, the exotic resonance is produced preferably from spin triplet states.

Figure 7. Dalitz plot for $\bar{p}p \to \pi^0\pi^0\eta$ obtained with a gaseous hydrogen target at 12 atm (2 entries per event).
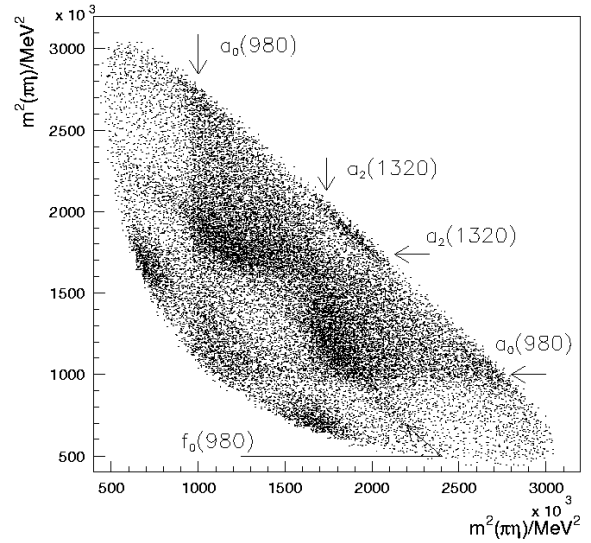
References

1. A. Abele et al., Phys. Lett. **B423** (1998) 175.
2. A. Abele et al., Phys. Lett. **B446** (1999) 349.
3. D. Alde et al., Phys. Lett. **B205** (1988) 397.
4. G.M. Beladidze et al., Phys. Lett. **B313** (1993) 276.
5. D.R. Thompson et al., Phys. Rev. Lett. **79** (1997) 1630.
6. G. Adams et al., Phys. Rev. Lett. **81** (1998) 5760.
7. A. M. Zaitsev, Proc. XXII. Int. Workshop on High Energy Physics and Field Theory (Protvino 1999) 7.
8. S.M. Flatté, Phys. Lett. **B63** (1976) 224.
9. Calculations by K. Hüttmann (MPI f. Physik, Munich).